Desalination and Water Treatment
www.deswater.com

doi: 10.5004/dwt.2022.28801

274 (2022) 102–114
October

Effect of H_3PO_4 oxidation of corn cob biochar on the adsorption of a commercial glyphosate formulation

Nayara Valeria Assis Marcelino, Hellem Victoria Ribeiro dos Santos, Renata Medici Frayne Cuba, Francisco Javier Cuba Teran*

Federal University of Goiás (UFG), Goiânia 74605-220, Brazil, emails: paco@ufg.br (F.J. Cuba Teran), nayara.valeria@hotmail.com (N.V. Assis Marcelino), hellemvsantos@gmail.com (H.V. Ribeiro dos Santos), renatafrayne@ufg.br (R.M. Frayne Cuba)

Received 17 January 2022; Accepted 5 August 2022

ABSTRACT

The adsorption of commercial glyphosate on biochar (BC) and oxidized biochar (BCox) from corn cob was studied thoroughly to characterize in detail the behavior of these adsorbent materials. Kinetic, isothermal and thermodynamic tests were performed in both materials using Brunauer–Emmett–Teller surface area analysis, accelerated surface area and porosimetry, Fourier-transform infrared spectroscopy, Barrett–Joyner–Halenda pore size and volume analysis, X-ray diffraction and scanning electron microscopy techniques. Adsorption equilibrium occurred in 60 min with an adsorption capacity of 0.58 $mg \cdot g^{-1}$ (22.3%) for BC and 1.49 $mg \cdot g^{-1}$ (53.2%) for BCox, with the latter showing a higher adsorption rate in the initial stage, reaching a 44% removal in the first 5 min, while in the case of BC, the removal was 5%. The pseudo-first-order kinetic model better adjusted to both adsorbents, although in the case of oxidized biochar, the Avrami model suggested that adsorption can also occur according to the pseudo-second-order model. Experimental data fitted in Langmuir and Freundlich isotherms revealed a more accurate fitting with the Freundlich model. The thermodynamic analysis showed that the adsorption of glyphosate was an endothermic and nonspontaneous phenomenon in this study. Acid oxidation with H_3PO_4 produced smaller pores and caused the collapse of the porous structure of the adsorbent. The results also showed that although acid oxidation enhanced the adsorption of commercial glyphosate, the values were considered low when compared with those obtained for pure compounds presented in the literature.

Keywords: Acid oxidation; Herbicide; Adsorbent materials

1. Introduction

Glyphosate (N-phosphonomethylglycine/$C_3H_8NO_5P$) is a nonselective, postemergent and systemic herbicide [1]. Even when used directly in the soil, the compound reaches the underground and surface waterbodies by means of surface transport and leaching. Osten and Dzul-Caamal [2] detected the presence of glyphosate in groundwater and surface water at concentrations between 0.44 to 1.41 $\mu g \cdot L^{-1}$ and 0.35 to 0.65 $\mu g \cdot L^{-1}$, respectively.

Adsorption is a physical–chemical treatment technique widely used for the removal of organic contaminants in water and wastewater due to its efficiency, ease of design and operation [3] and for not being affected by compounds with potential toxicity [4]. However, the costs involved in the production of activated carbon limit its use to a large proportion [5]. Thus, studies aimed at the use of biochar as an alternative material to activated carbon have been intensified in recent times.

* Corresponding author.

Biochar is a carbon-rich solid material obtained from the thermal or hydrothermal decomposition of organic material under limited oxygen conditions [6] and relatively low temperatures (350°C–700°C) [7]. Different materials are presented in the literature as precursors of biochar, among which there are those of lignocellulosic origin as agricultural residues that also confer environmental benefits to the process due to the valorization of these materials [8]. The corn cob has adequate biomass composition for its conversion into biochar, with 40.95% cellulose, 38.94% hemicellulose and an insignificant amount of lignin (16.54%) [9].

Biochar produced from corn cobs has been widely used to remove organic contaminants present in water. Dibutyl phthalate and di(2-ethylhexyl) phthalate removal of 16.16 and 13.2 $mg \cdot g^{-1}$, respectively [10], brilliant green dye removal of 16.53 $mg \cdot g^{-1}$ [11] and methylene blue removal of 16.50 $mg \cdot g^{-1}$ [12] are some of the examples.

According to Wang and Wang [13], the adsorption capacity of biochar is directly associated with its physical–chemical properties, such as surface area, pore distribution and size, and the presence of functional groups. However, the pyrolysis conditions commonly used for the preparation of biochar do not allow the proper development of these characteristics, reducing the efficiency of the adsorption process [14].

Changes in the surface structure of biochar to improve adsorption capacity can be achieved through chemical or physical activation, and chemical activation is the most common method due to mild activation conditions and high yields generally obtained [15]. In chemical activation, the precursor material or biochar is doped with a chemical agent and subjected to high temperatures, usually between 450°C and 750°C [15], altering its porosity and surface area as a result of dehydration and oxidation of the material [16]. Different chemical compounds can be used as activating agents, among which phosphoric acid (H_3PO_4) stands out due to its low corrosiveness, lower costs and lower pollutant characteristics [17].

Meng et al. [18] oxidized biochar produced from cotton bark with H_3PO_4 (350°C) and obtained a specific surface area and total pore volume 114 and 22.7 times higher than those obtained for biochar without oxidation, respectively. Chu et al. [17] studied biochar treated with H_3PO_4 (500°C and 650°C) and observed an increase both in the surface area and in the total volume of pores, classified as micropores (<2 nm), which contributed to the adsorption of organic compounds. Ma et al. [19] increased the surface area of the biochar produced from sewage treatment plant sludge by approximately 3 times after acid activation at a temperature of 450°C.

However, studies have shown that acid oxidation and low temperatures have also modified and improved the surface characteristics and adsorption capacity of biochar, as they create hydrophilic functional loads and groups on the surface of oxidized material [20]. Sen et al. [21] impregnated biochar produced from eucalyptus bark with H_3PO_4 6N at 60°C and obtained an adsorbent with a surface area of 0.54 $m^2 \cdot g^{-1}$. Iqbal et al. [22] treated biochar produced from Sidr (Ziziphus spina-christi) dead leaves with H_3PO_4 0.5 M (room temperature) and observed that the surface area and pore volume for the modified biochar were 6.0873 $m^2 \cdot g^{-1}$ and 0.01034 $cm^3 \cdot g^{-1}$, respectively, which resulted in an increase of 1.4 times in the adsorption capacity of the modified biochar when compared to the capacity of the biochar without modification.

Farhaneem et al. [23] used variance analysis (ANOVA) to verify the influence of the H_3PO_4 concentration (0.5 M) and temperature (70°C, 80°C and 90°C) on the surface properties of biochar produced from rubber wood sawdust and concluded that the increase in acid concentration resulted in a higher surface negative load due to the greater presence of acidic functional groups and, as a countermatch, they found that variations in oxidation temperature did not produce significant effects on the process.

Although it is shown in the literature that the oxidation of biochar with acidic substances at low temperatures is able to promote desirable surface characteristics for the removal of organic contaminants in aqueous media, studies are still scarce, so there is little information about the materials produced and the predominant adsorption mechanisms. Additionally, in regard to glyphosate adsorption in biochar, pure compounds were used [24–26], and there is a lack of information in regard to commercial products that contain additional compounds in their formulation, such as surfactants, which may influence the adsorption process due to co-adsorption in the adsorbent material [27].

Thus, the present study aims to verify the removal of glyphosate (commercial formulation) in aqueous medium by adsorption in biochar produced from corn cobs subjected to acid oxidation at 60°C.

2. Experimental approach

2.1. Reagents used

The glyphosate solution (GLP) used was obtained from the commercial product Roundup® Original DI (Monsanto), consisting of diammonium salt of N-(phosphonometil) glycine (445 $g \cdot L^{-1}$), equivalent to *n*-acid (phosphonometil) glycine (370 $g \cdot L^{-1}$). The other reagents used were of analytical grade (neon), and the solutions were prepared with deionized water.

2.2. Preparation of adsorbent materials

For the production of adsorbent materials, corn cobs were cut into cubic shapes with dimensions equal to 1 cm and then dried in an oven at 105°C for 24 h to eliminate water content.

The dry material was transferred to porcelain capsules that were encased in aluminum foil to obtain an atmosphere with an oxygen deficit [28]. To allow the output of volatilized compounds from the inside of the capsules during carbonization, small holes were made on the surface of the foil. Carbonization was carried out in a muffle oven (Quimis) at a temperature of 500°C for 3 h [27]. The biochar (BC) obtained was washed with ultrapure water for removal of ash and macerated manually.

Oxidation was performed by keeping BC in phosphoric acid solution (H_3PO_4 – 6N) at a ratio of 1:3 (BC:H_3PO_4) for 24 h at 60°C and then neutralizing with sodium hydroxide

(NaOH – 0.1N). Oxidized biochar (BCox) was washed with methanol (20%), deionized and dried water in an oven at ±105°C [21].

The biochar produced was stored in polyethylene bottles at room temperature.

2.3. Physicochemical analyses

GLP analyses were performed according to the method proposed by Tzaskos et al. [30] consisting of mixing 5 mL of the sample in 0.5 mL of ninidrin (5%) and 0.5 mL of sodium molybdate (5%). The mixture was heated in a water bath (Tecnal – TE057) for 12 min at 92°C ± 1°C for the formation of Ruhemann's purple product, with maximum absorption at 570 nm. Prior to GLP analysis, the samples were filtered in a fiberglass membrane (0.47 μm) with the aid of a vacuum pump system. GLP concentration readings were performed on a Hach DR 5000 spectrophotometer.

The calibration curve (coefficient of determination R^2 = 0.9909) was constructed using dilutions prepared from the commercial solution used in the tests. This procedure was chosen to avoid possible interference of other constituents present in the commercial formulation when compared to the pure product.

The determination of pH values was performed by a potentiometric method using a digital pH meter (Tecnal).

2.4. Physico-chemical characterization of BC and BCox

The granulometric analysis was performed using a set of graduated sieves belonging to the Tyler series (Bertel) [31]. The zero-point-charge pH value (pH_{zpc}) was determined by the 11-point method [32].

The surface and textural properties were determined from the nitrogen adsorption–desorption isotherms (N_2) (–196°C) using Micromeritics ASAP (accelerated surface area and porosimetry) 2020 equipment. The surface area (S_{BET}) was determined by the B.E.T. method, and the total pore volume (V_T) was obtained by desorption isotherm from the volume of N_2 desorbed at a relative pressure (P/P_0) of 0.95; the distribution and the average diameter of the pores (D_P) were determined by the Barrett–Joyner–Halenda method.

The crystallographic properties were determined by X-ray diffraction (Bruker D8 Discover diffractometer). The morphology and elementary surface composition were determined by scanning electron microscopy (SEM) and dispersive energy spectroscopy (EDS), respectively. The functional groups on the surface of BC and BCox before and after glyphosate application were analyzed using Fourier-transform infrared spectroscopy (FTIR; PerkinElmer spectrometer, Spectrum 400).

2.5. Glyphosate adsorption experiments – commercial formulation (GLP) in BC and BCox

To evaluate the adsorption in BC and BCox, pH, mass, velocity, capacity and thermodynamic adsorption parameters were determined. All tests were performed in batch reactors under constant agitation of 120 rpm in an orbital agitator table (Solab SL-180/A) maintained in an air-conditioned chamber with temperature control (Alfa Mare, AM – 581 A). The GLP solutions were prepared from stock solutions with a concentration of 500 mg·L^{-1}.

To determine the effect of pH on adsorption, 0.5 g adsorbent (BC and BCox) was suspended in 50 mL of GLP solution with pH previously adjusted to the values of 1.5, 2.5, 4.0, 7.0 and 11 using solutions of HCl or NaOH both 0.1 M. pH values were adopted taking into account the pK_b and pK values of the glyphosate molecule pK_b < 2, pK_{a1} = 2.27, pK_{a2} = 5.57 and pK_{a3} = 10.86. The adsorbent mass was determined by suspending 0.25, 0.5, 0.75, 1.0 and 1.5 g of adsorbent in GLP solution with the pH value previously obtained in adsorption tests. In both assays, the concentration of GLP solutions used was 12 mg·L^{-1} at room temperature (23°C ± 2°C) for 24 h. The values were defined from studies on glyphosate adsorption available in the literature [21,33].

To determine the GLP concentration, after the experimental period, the samples were filtered through 0.47 μm fiberglass membranes, and the residual GLP concentration was determined. The analyses were performed in triplicate and with blank samples for each pH and adsorbent mass.

The percentage of removal and the adsorption capacity of GLP were determined by applying Eqs. (1) and (2):

$$\%R = \frac{\left(C_0 - C_{eq}\right) \times 100}{C_0} \tag{1}$$

$$q_{eq} = \frac{\left(C_0 - C_{eq}\right) \times V}{m} \tag{2}$$

where $\%R$ is the percentage of removal, q_{eq} is the ability of adsorption in balance (mg·g^{-1}), C_0 is the initial concentration of GLP (mg. L^{-1}), C_{eq} is the concentration of GLP in equilibrium (mg·L^{-1}), V is the volume of the solution (L) and m is the mass of BC or BCox (g).

The pH and adsorbent mass conditions that provided the best performance were used for thermodynamic, capacity and adsorption kinetics assays.

2.6. Kinetic and adsorption isotherm assays

The kinetic adsorption parameters for BC and BCox were obtained in batch assays using 50 mL of GLP solution with an initial concentration of 12 mg·L^{-1} and 0.25 g adsorbent at pH 7.0.

The vials with the solutions were kept under constant agitation at a temperature equal to 23°C ± 2°C, and at predetermined intervals, aliquots were collected to determine the GLP concentration until equilibrium.

The data obtained in the kinetic study of GLP adsorption were adjusted to the pseudo-first-order, pseudo-second-order [24], Avrami [34] and Weber–Morris models based on the intra diffusion particle model [35], according to Eqs. (3)–(6), respectively.

$$q_t = q_e\left(1 - e^{-k_1 t}\right) \tag{3}$$

$$q_t = \frac{q_e^2 k_2 t}{1 + k_2 q_e t} \tag{4}$$

$$q_t = q_{av}\left(1-\exp\left(-K_{av}t\right)^n\right)\right) \quad (5)$$

$$q_t = k_i t^{1/2} + C \quad (6)$$

where q_{eq} and q_{av} are the theoretical adsorption capacity of GLP per adsorbent mass (mg·g^{-1}) for the pseudo-first-order and pseudo-second-order and Avrami models, respectively; q_t amount of adsorbed GLP (mg·g^{-1}) in time t (min); n is the fractional order of reaction that may be related to the adsorption mechanism; k_1 (min^{-1}), k_2 (g·mg^{-1}·min^{-1}), k_{av} (min^{-1}) and k_i (mg·g^{-1}·h$^{-0.5}$) are the constants of the adsorption rates of the 4 kinetic models, respectively; and C (mg·g^{-1}) is a constant, which represents the boundary layer of the adsorbent.

To perform the adsorption isotherm assay, 0.25 g of BC and BCox was added to 50 mL of GLP solution at concentrations of 2.5, 5, 10, 15, 20 and 25 mg·L^{-1}. The flasks were kept under constant agitation for 24 h at temperatures equal to ±23°C, ±43°C and ±63°C.

The nature of the GLP adsorption process was determined by adjusting the data obtained at 23°C to the Langmuir and Freundlich models [Eqs. (7) and (8)] [24].

$$q_e = \frac{q_{max}K_L C_{eq}}{1+K_L C_{eq}} \quad (7)$$

$$q_e = K_f C_{eq}^{1/n} \quad (8)$$

where C_{eq} is the concentration of GLP in balance (mg·L^{-1}); q_{eq} is the ability of adsorption in balance (mg·g^{-1}); K_L (L·mg^{-1}) is an adsorbate–adsorbent interaction constant that, when it assumes high values, indicates strong adsorbent affinity for adsorbent sites; q_{max} is the maximum adsorption capacity (mg·g^{-1}), which represents the total number of sites available in the adsorbent material; K_F [(mg·g^{-1})(L·mg^{-1})$^{1/n}$] and n are Freundlich constants that relate, respectively, to adsorption capacity and intensity.

Parameter n indicates whether adsorption is favorable, being favorable when it assumes values from 1 to 10. The higher the value of this parameter is, the greater the adsorbate–adsorbent interaction. Furthermore, it is possible to express the essential characteristics of Langmuir's isotherm in terms of the separation factor R_L, calculated using Eq. (9).

$$R_L = \frac{1}{1+R_L C_i} \quad (9)$$

where C_i is the highest initial concentration of adsorbate (mg·L^{-1}) and R_L is used for the interpretation of the adsorption process: irreversible process ($R_L = 0$), favorable ($0 < R_L < 1$), linear ($R_L = 1$) or unfavorable ($R_L > 1$) [36].

From the adsorption isotherms of GLP (q_{eq} vs. C_{eq}), the thermodynamic equilibrium constant K_D was calculated using the graph of $\ln(q_{eq}/C_{eq})$ vs. q_{eq}, extrapolating to $q_{eq} = 0$. With the values of K_D for each temperature, the values of $\Delta S°$ and $\Delta H°$ were obtained by Eq. (10) and $\Delta G°$ by Eq. (11).

$$\ln\left(K_D\right) = \frac{\Delta S^\circ}{R} - \frac{\Delta H^\circ}{R.T} \quad (10)$$

$$\Delta G^\circ = -RT\ln\left(K_D\right) \quad (11)$$

where K_D is the thermodynamic equilibrium constant; ΔG, ΔS and ΔH are the free energy of Gibbs (kJ·mol^{-1}), entropy variation (J·mol^{-1}·K^{-1}) and enthalpy (kJ·mol^{-1}), respectively; R is the universal gas constant (8,314 J·mol^{-1}·K^{-1}), and T is the temperature (K) [10].

2.7. Statistical analyses

To evaluate the quality of the adjustments, the values of the coefficients of determination (R^2) and the chi-square test (x^2) were used as criteria. The x^2 test took into account the experimentally observed results and the values predicted by the model applying them in Eq. (12) used by Ho and Ho and Wang [37].

$$x^2 = \sum \frac{\left(q_{e.exp} - q_{e.m}\right)^2}{q_{e.m}} \quad (12)$$

where $q_{e,exp}$ is the experimental data of equilibrium ability (mg·g^{-1}) and $q_{e,m}$ is the equilibrium capacity calculated by the model (mg·g^{-1}). The difference between $q_{e,m}$ and $q_{e,exp}$ was also compared.

3. Results and discussion

3.1. Physical–chemical characterization of BC and BCox

Table 1 presents the results of the physicochemical characterization of BC and BCox.

The average diameter of the particles (arithmetic average of the sieve opening in which the solid plots were retained) was 0.07 mm for both BC and BCox. The S_{BET} value for BC was 4.5 times higher than that for BCox, and the pore volumes were 0.057293 and 0.038697 cm^3·g^{-1}, respectively. Guzel et al. [38] observed a reduction between 1.6 and 7.9 times in S_{BET} biochar after acid treatment with different concentrations of HNO_3 to 80°C due to either narrowing of the pore entrances of oxygen groups formed on the entrance and walls of pores. The reduction in V_T may have occurred because of the removal of porosity due to the collapse of the pore walls in the structure [38].

Fig. 1 shows photomicrographs obtained by SEM of BC (A and C) and BCox (B and D). A morphologically more homogeneous pore structure can be observed in BC, while in BCox, an irregular surface morphology with pores of different sizes and shapes is observed. The possible structure of the collapsed pore wall is highlighted (images B and D).

Regarding the format of the adsorption/desorption isotherms of N_2 (Fig. 2), the acid treatment did not change the format that exhibited type III classification according to the IUPAC. These types of isotherms are common in nonporous materials, and generally, in these cases, adsorbent–adsorbate interactions are weaker than adsorbate-adsorbate interactions [39].

The average pore size in BC was 35 Å and BCox 45 Å, equivalent to mesoporous solids [40]. Zhou et al. [41] explained that pyrolyzed materials at low temperatures

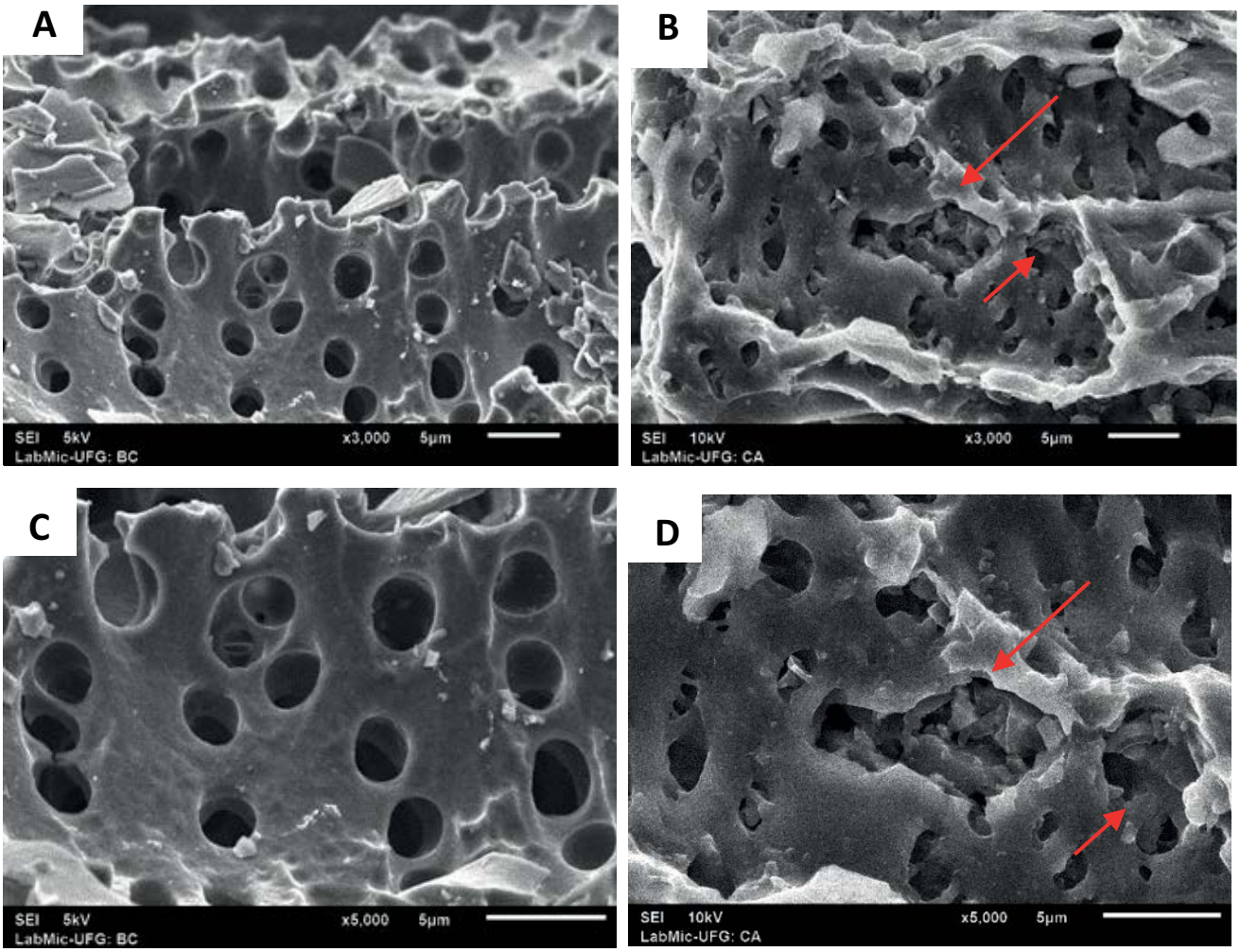

Fig. 1. Photomicrographs of BC and BCox samples.
Notes: (A, C) correspond to BC and (C, D) correspond to BCox. Magnification of resolution: A and B 3,000 times; C and D 5,000 times.

Table 1
Physical–chemical characterization of BC and BCox adsorbents

	Adsorbent	
Parameter	BC	BCox
Average particle diameter (mm)	0.07	0.07
pHpzc	8.0	8.0
Surface area (S_{BET}) ($m^2 \cdot g^{-1}$)	34.1261	7.4856
Total pore volume (V_T) ($m^3 \cdot g^{-1} \cdot cm$)	0.057293	0.038665
Typology	Mesoporous	Mesoporous
Morphology	Homogeneous surface	Heterogeneous surface
Elementary composition	C, O and K	C, O, Na and P
Crystalline structure	Solid amorphous	Solid amorphous

have a lower tendency to form micropores because the volatile material is not released from the biochar matrix. Ates and Öznur [42], when analyzing the effect of temperature and concentration of H_3PO_4 on biochar activation, concluded that H_3PO_4 (85%) in the ratio 2:1 and 500°C was the ideal condition for obtaining a biochar with the best conditions for micropore formation, acid concentration conditions and temperature well above those used in this article.

Fig. 3 shows the elemental composition present on the surface of BC and BCox.

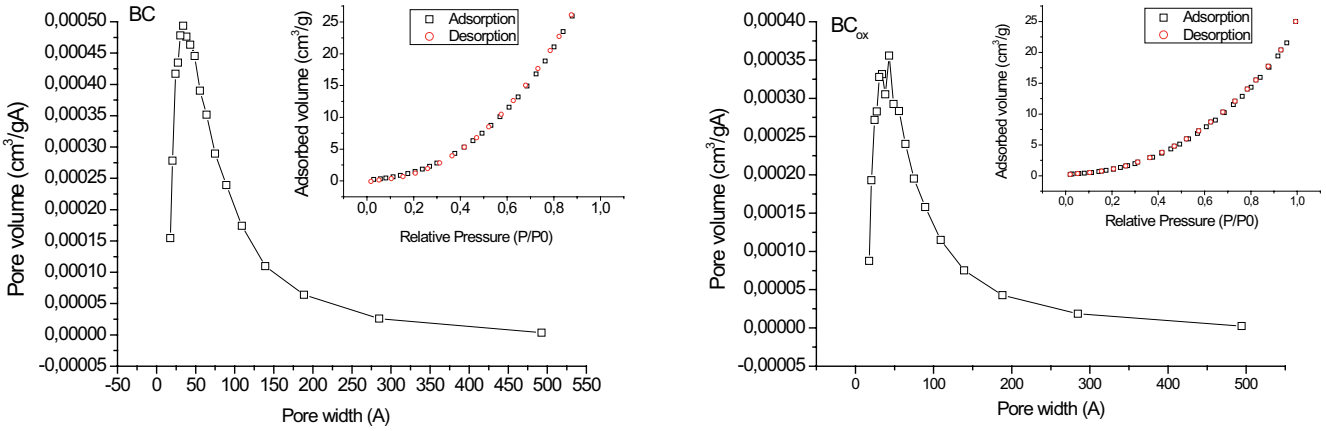

Fig. 2. Adsorption/N2 desorption isotherms for BC and Bcox and the distribution of pore sizes.

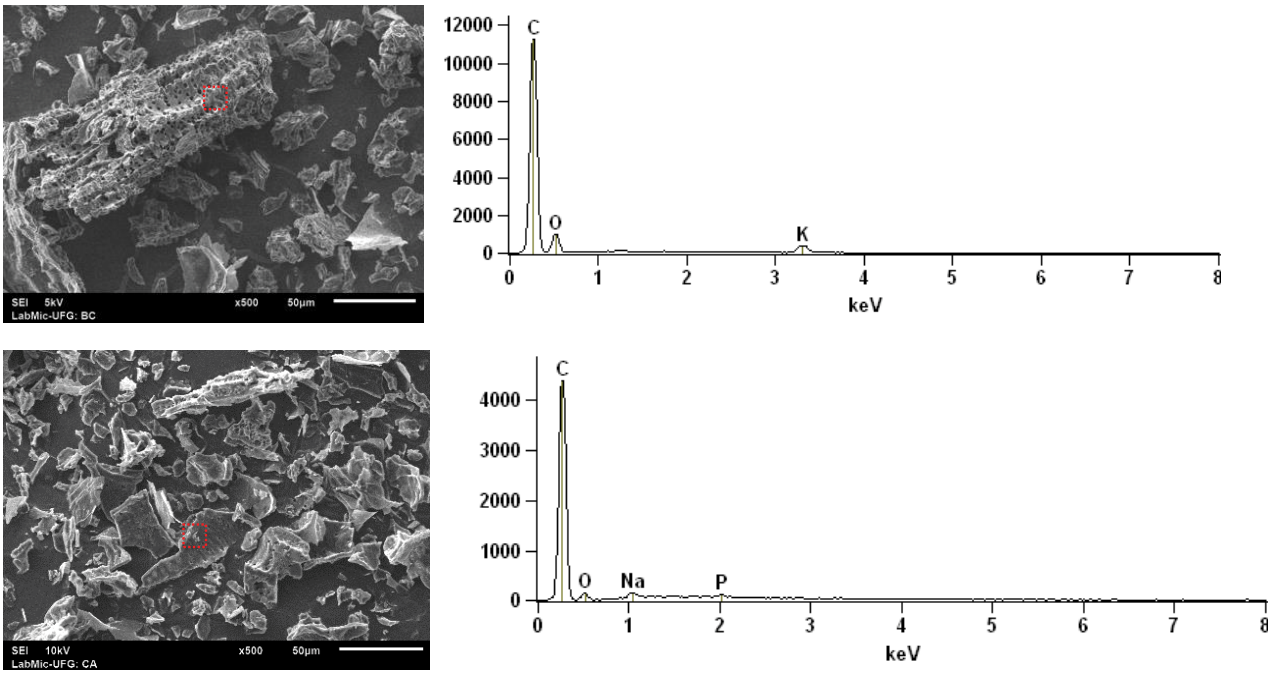

Fig. 3. Dispersive energy spectroscopy of BC and BCox.

In both adsorbents, there is a predominance of carbon (C) since, for the analyzed points, no impurity or compost presented significant peaks. On the surface of BC, the presence of potassium (K) is observed, possibly due to the chemical composition of the corn cob and the carbonization that did not volatilize this inorganic compound. In BCox, the presence of phosphorus (P) and sodium (Na) was detected, the first probably due to remnants of the oxidation process and the second of neutralization with sodium bicarbonate solution ($NaHCO_3$).

There were no significant changes in relation to the position of the peaks in 2θ after acid treatment. Both adsorbents have diffuse patterns, indicating their amorphous nature. Two wide diffraction peaks were verified between 2θ = 25° and 45°, confirming the formation of typical activated carbon structures [43].

The pH_{zpc} also remained stable at 8.0 for BC and BCox. Thus, for pH < 8.0, the surface becomes positively charged due to adhesion of H^+ ions on the surface. However, at higher pH values, the surface is negatively charged due to OH^- ions [21].

3.2. GLP adsorption tests

3.2.1. Effect of the initial mass of BC and BCox

The removal (%) and the adsorption capacity (q_e) of GLP as a function of the adsorbent mass are presented in Fig. 4.

The highest GLP removals occurred for a mass of 0.5 g adsorbent, 62.7% for BCox and 48.9% for BC. Regarding adsorption capacity, the best performance for both adsorbents was verified for a mass of 0.25 g (833:1 GLP:adsorbent)

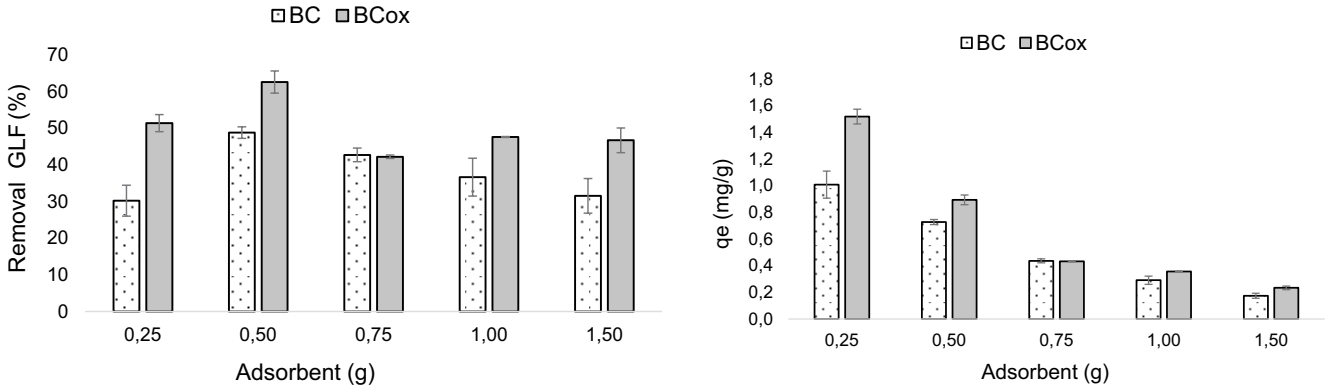

Fig. 4. Removal and GLP adsorption capability as a function of adsorbent mass.

Notes: Orbital agitation at 120 rpm, 24 h, C_0 = 12 mg·L^{-1}, pH = 7.0, variation of adsorbent ratio (mg) and GLP (mg), present in the solution, of 416:1; 833:1; 1,250:1; 1,666:1; 2,500:1, 50 mL solution, temperature of 23°C, triplicate.

being 1.52 and 1.00 mg·g^{-1} for BCox and BC, respectively. The acid treatment results in an increase in surface acidic functional groups such as carboxylic, lactone and phenol groups [38] that can act as H-donor and acceptor groups, forming strong H-bonding with the glyphosate molecule [44].

The decrease in adsorption capacity (q_e) with the increase in mass occurs because the addition of available surface area does not result in increased adsorption, since there is interference between the adsorbent binding sites [45].

3.3. Effect of pH

At pH values up to 7.0, adsorption increased for both adsorbents, with a maximum of 0.70 mg·g^{-1} (47.9% removal) for BC and 0.91 mg·g^{-1} (67.8% removal) for BCox. After that, the removal decreased drastically. Similar behavior was reported by Mayakaduwa et al. [24], but with a maximum adsorption capacity of 21.6 mg·g^{-1}; however, the authors used glyphosate of analytical grade (98%).

Fig. 5 shows the GLP adsorption capacity (mg·g^{-1}) for BC and BCox and the predominance of dissociated forms of the GLP molecule as a function of pH.

The lower GLP removal capacity for pH values away from neutrality may be associated both with the surface loads of adsorbents as well as with the degree of ionization and speciation of the GLP molecule [46]. The pHpzc for BC and BCox was 8.0. Thus, at pH values = 7.0, the surfaces of adsorbents become positively charged, exhibiting strong tendencies to electrostatic interactions with negatively charged groups of GLP molecules that predominate at pH close to neutrality. For pH > 8.0, the density of negative charges on the adsorbent surface and the predominance of negatively charged glyphosate species (C and D) increase, causing electrostatic repulsion between the adsorbate and adsorbent and consequently a decrease in GLP adsorption [44].

3.4. Superficial functional groups

The spectra presented in Fig. 6A suggest that the corn cob underwent complete carbonization since bands of 2,900 cm^{-1} could not be identified, characteristic of the C–H stretch of aliphatic compounds [29]. It can also be verified

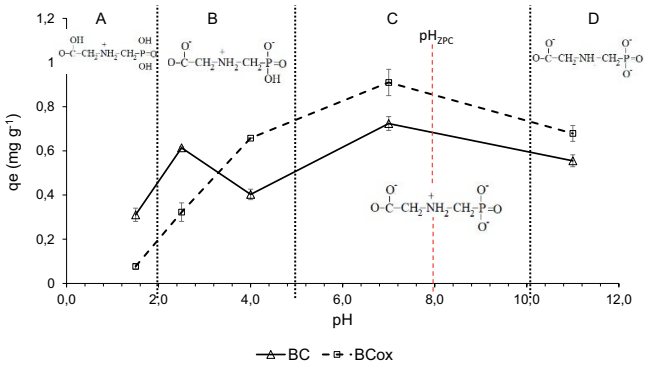

Fig. 5. GLP adsorption capacity as a function of pH and dissociated forms of GLP molecules at different pH intervals for BC and BCox.

Notes: Orbital agitation at 120 rpm, 24 h, C_0 = 12 mg·L^{-1}, mass ratio (mg) and volume (mL) of 10:1 (0.5 g) (adsorbent mass/solution volume), 50 mL solution, temperature of 23°C, triplicate.

that oxidation with H_3PO_4 did not promote the formation of new functional groups on the surface of the adsorbent material, since it is possible to identify absorption peaks in the same regions of the spectrum before and after oxidation. Furthermore, the absence of a narrow peak close to 1,642 cm^{-1} (Fig. 6A–C) demonstrates the absence of physically adsorbed water [44].

The bands present between 880 and 750 cm^{-1} are observed when there is deformation outside the c-h connection plane for different substitutions in the benzene ring, while the small peaks near 1,700 (1,692 cm^{-1}) are characteristic of vibrational frequencies of stretches of C=O bonds present in ketones, aldehydes, lactones or carboxyl groups (Fig. 6C) [47].

The bands at 3,381 cm^{-1} (Fig. 6B and C) are characteristic of stretches of hydrogen bonds (–O–H) of hydroxyl groups [48] present in carboxyles, phenolic hydroxyls, alcohols or water absorbed in the adsorbent [17]. After activation, this peak increased in intensity (Fig. 6A), suggesting that superficial groups containing functional oxygen increased [49]. The increase in functional groups

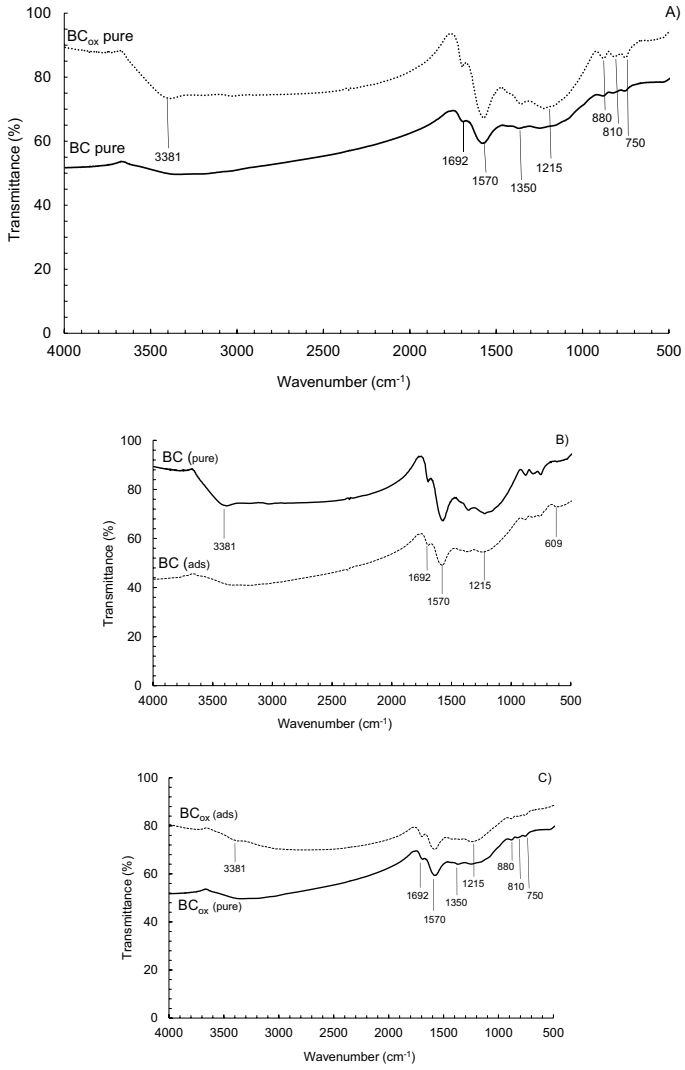

Fig. 6. Infrared spectra of BC and BCox without adsorption of GLP (A) and spectra before and after GLP adsorption for BC (B) and BCox (C).
Notes: Comparison of the spectra obtained for (A) BC and BCox without GLP adsorption, (B) BC before adsorption (BC_{pure}) and BC after adsorption (BC_{ads}) and (C) BCox before adsorption ($BCox_{(pure)}$) and after GLP adsorption ($BC_{(ads)}$).

containing oxygen may contribute to the adsorption of GLP due to the possibility of hydrogen bond formation. Fig. 6C shows the decrease in peak intensity at 1,692 cm^{-1} attributed to changes in carboxylic groups [50], which according to Herath et al. [44] may be due to the formation of strong hydrogen bonds with GLP molecules.

To explore the possibility of increasing superficial functional groups in BCox, the amount of adsorbate was expressed per unit of area (mg·m^{-2}) [10]. The results show that even though BCox has a smaller surface area than BC, the amount of GLP adsorbed per unit of area was higher, 0.017 and 0.20 mg·m^{-2}, respectively, suggesting that the functional groups formed contributed to GLP adsorption [52].

3.5. Adsorption kinetics

For both adsorbents, there is a fast and a slow phase for the adsorption mechanism (Fig. 7). This phenomenon occurs due to the progressive occupation of active adsorption sites becoming saturated with contact time [53].

The equilibrium was reached in the first hour of the test with an adsorption capacity of 0.58 mg·g^{-1} (22.3%) for BC and 1.49 mg·g^{-1} (53.2%) for BCox. This phenomenon can occur, where active sites do not fill; then, the collision rate between the adsorbate and adsorbent increases, where a concentration of glyphosate molecules is present in a large number of available sites [21]. However, active sites tend to become progressively saturated, perhaps due to the electrostatic hindrance between the adsorbed negatively charged adsorbate species and the surface, resulting in a slow rate of adsorption of glyphosate onto the bulk of the adsorbent [44].

The fitting of the results to the kinetic models demonstrates that both BC and BCox presented adequate adjustments for the three models adopted. The values of R^2 and x^2 obtained and the difference between experimental

q_e ($q_{e,exp}$) and q_e calculated by the model ($q_{e,calc}$) presented in Table 2 suggest that for BC, the pseudo-first-order model was better adapted, and this result was confirmed by the Avrami model, whose value of n = 0.9673 was very close to 1.

For BCox, although the statistical parameters (R^2 = 0.9987 and x^2 = 0.0097) indicate correspondence with the pseudo-second-order model, Avrami's model also had a good fit (R^2 = 0.98963 and x^2 = 0.00132), indicating that GLP adsorption also follows the pseudo-first-order model, in view of the value of n (0.59716) being closer to 1 [34].

According to Mayakaduwa et al. [24] in the pseudo-first-order model, the process is considered a non-dissociative molecular adsorption. Furthermore, adsorbate removal occurs due to the difference in adsorbate concentration between the adsorbent surface and the solution, occurring only when the mass transfer coefficient controls the process [34]. The pseudo-second-order model assumes that adsorbate removal is a multistep process that involves sorption on the surface and diffusion in the adsorbent prevailing reactions involving valence forces or electron exchange between the adsorbate and adsorbent [54].

Thus, although there is an adequate adjustment for the pseudo-first-order and pseudo-second-order models, both in BC and BCox, GLP adsorption is controlled by the external mass transfer coefficient and dependent on the initial concentration of GLP [44].

Furthermore, according to the parameters obtained, the adsorption ability in equilibrium (q_e) of BCox was 2.6 times higher than that of BC. This behavior was also obtained by Magid et al. [10] when studying the adsorption of phthalates in corncob biochar without and with acid treatment.

The values of k_1 for the BC of 0.06361 min^{-1} and for the BCox of 0.34698 min^{-1} (~5.4 times greater) confirm the higher rate of GLP adsorption in the BCox observed in the graphs of Fig. 7, where it was verified that 44% of the removal of glyphosate by BCox occurred in the first 5 min, while for BC removal for the same period, it was 5%.

To identify the stages of adsorption of GLP in BC and BCox, the application of the intraparticle diffusion model was used in the method proposed by Weber–Morris, in

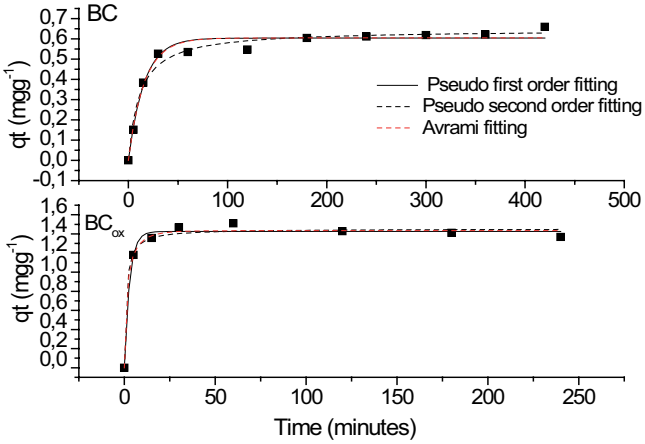

Fig. 7. Influence of kinetic contact time and adjustment of adsorption data for BC (A) and BCox (B).
Notes: Orbital agitation at 120 rpm, 4 h, C_0 = 12 mg·L^{-1}, 0.25 g (5:1) adsorbent mass, 50 mL solution, samples taken at times of 0, 5, 15, 30, 60, 120, 180 and 240 min, temperature of 23°C, pH equal to 7.0, triplicate.

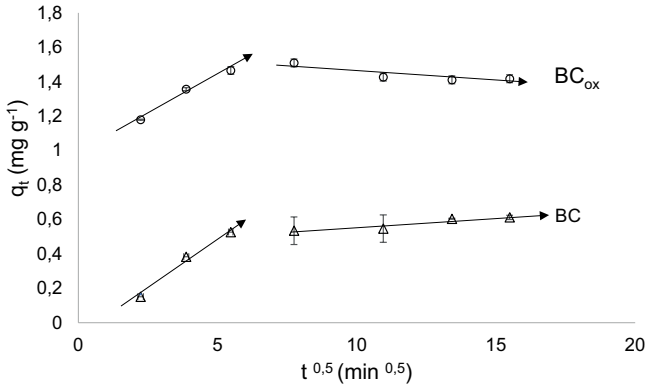

Fig. 8. Adjustment of the kinetic data of GLP adsorption in BC and BCox. Weber–Morris method.
Notes: Orbital agitation at 120 rpm, 4 h, C_0 = 12 mg·L^{-1}, 0.25 g (5:1) adsorbent mass, 50 mL solution, samples taken at times of 0, 5, 15, 30, 60, 120, 180 and 240 min, temperature of 23°C, pH equal to 7.0, triplicate.

Table 2
Kinetic parameters of pseudo-first-order, pseudo-second-order and Avrami models for GLP adsorption in BC and BCox

Adsorbent	$q_{and\ exp}$	Pseudo-first-order	Pseudo-second-order	Avrami
BC	0.58	$q_{eq,calc}$ = 0.60373 k_1 = 0.06361 R^2 = 0.97457 x^2 = 0.0018	$q_{eq,calc}$ = 0.64583 k_2 = 0.13766 R^2 = 0.97899 x^2 = 0.0097	q_{av} = 0.6046 k_{av} = 0.0630 n = 0.9673 R^2 = 0.97139 x^2 = 0.00132
BCox	1.49	$q_{eq,calc}$ = 1.42483 k_1 = 0.34698 R^2 = 0.98939 x^2 = 0.00266	$q_{eq,calc}$ = 1.45261 k_2 = 0.64908 R^2 = 0.9987 x^2 = 0.00308	q_{av} = 1.43395 k_{av} = 0.49165 n = 0.59716 R^2 = 0.98963 x^2 = 0.00262

Notes: $q_{eq,calc}$ = mg·g^{-1}; k_1 = min^{-1}; k_2 = g·mg^{-1}·min^{-1}; q_{av} = mg·g^{-1}); n = min^{-1}.

which the adsorption capacity data of GLP (q_t) at different times (t) were plotted as a function of $t^{0.5}$ [55], whose results are shown in Fig. 8.

The results in Fig. 8 present multilinearity, which suggests the occurrence of different stages of adsorption, and each stretch represents a distinct mechanism of mass transfer [34]. In the first linear stretch, there is the fastest stage of adsorption (~30 min), where external mass transfer occurs in which the GLP molecule is transported to the surface of the adsorbents (BC and BCox) due to the strong electrostatic attraction between the adsorbate and adsorbent.

The second section, in which a gradual adsorption of GLP is identified, is controlled by intraparticle diffusion, which occurs after adsorbent sites of the adsorbent are saturated [56]. Furthermore, the fact that no segment passes through the origin indicates that intraparticle diffusion is not the limiting step in the adsorption process but other mechanisms involved, which may even be operating simultaneously [57].

3.6. Adsorption isotherms for BC and BCox

Adsorption isotherms refer to the relationship, in equilibrium, between adsorbed concentration in aqueous solution and adsorbent capacity. The data obtained for both BC and BCox show that with the increase in the initial concentration of GLP, the adsorption capacity for both adsorbents also increases gradually. Zhang et al. [58] explained that this phenomenon can occur due to the driving force resulting from the concentration gradient and the greater opportunities to capture GLP molecules by the adsorbent as a function of the increase in GLP concentration.

The capacity and adsorption for BC and BCox were estimated by applying the Langmuir and Freundlich adsorption isotherm models to the GLP adsorption data obtained at a temperature of 23°C. Fig. 9 shows the results obtained for BC and BCox and the adjustments of the Langmuir and Freundlich isotherm models.

For BC, the Langmuir model (R^2 = 0.99863) was the one that best adjusted to the GLP adsorption data when compared to the Freundlich model (R^2 = 0.929). For BCox, only the Freundlich model (R^2 = 0.94715) could be adjusted.

Langmuir's model suggests that the adsorption mechanism is governed by chemosorption phenomena with a uniform distribution (monolayer adsorption) of adsorbate molecules on the adsorbent surface [58]. The Freundlich model indicates multilayer physical adsorption on an energetically heterogeneous surface [44].

In the case of BC, satisfactory adjustment for both models suggests that adsorption occurs through chemo- and physiosorption mechanisms. The data of the GLP adsorption parameters obtained for BC and BCox are shown in Table 3.

In the Langmuir model, the value and $R_L < 1$ obtained for BC represents that the adsorption of GLP on the adsorbent is favorable and the process is feasible, and for BCox, the value of n between 1 and 10 indicates a strong interaction between the adsorbate and adsorbent [26].

Thus, based on the results of kinetic models and isotherms as well as FTIR results and the pH conditions used in the study, it is suggested that GLP adsorption in BC and BCox occurred through physical interactions, being: a) π^+–π interactions of protonated amino groups (NH_2^+) of the glyphosate molecule with double bonds of aromatic rings on the surface of adsorbents and b) hydrogen bonds between groups GLP phosphate (P=O) and hydroxyls of phenolic and carboxylic groups of adsorbent surface and finally c) chemical interactions between positively charged groups on the surface of adsorbates (study pH < pHpzc) and negatively charged oxygens of the GLP molecule [26].

Table 3
GLP adsorption parameters for BC and BCox obtained from the adjustment to the Langmuir and Freundlich models

Isothermal model	Parameters	Adsorbent	
		BC	BCox
Freundlich	K_F	0.24779	0.08852
	n	1.65068	0.6911
	R^2	0.929	0.94715
Langmuir	q_{max}	0.28153	–
	K_L	7.53172	–
	R^2	0.99863	–
	L_R	0.01–0.06	–

3.7. Adsorption thermodynamics

The results of thermodynamic parameters, Gibbs free energy ($\Delta G°$), enthalpy ($\Delta H°$) and entropy ($\Delta S°$) of GLP adsorption in BC and BCox are shown in Table 4.

Table 4
Thermodynamic parameter of GLP adsorption in BC and BCox

Adsorbent	Thermodynamic parameters				
	T (°C)	K_D	ΔG (kJ·mol^{-1})	ΔH (kJ·mol^{-1})	ΔS (J·mol^{-1}·K^{-1})
BC	23	0.114	5.34	14.91	–70
	43	0.056	7.62		
	63	0.055	8.04		
BCox	23	0.177	4.25	21.70	60
	43	0.120	5.58		
	63	0.077	7.16		

Positive values of ΔH are observed, which indicate an endothermic nature of the GLP adsorption process; that is, the adsorbed amount increases with increasing t temperature for both adsorbents. The ΔH values obtained for BC (14.91 kJ·mol^{-1}) and BCox (21.70 kJ·mol^{-1}) are outside the $\Delta H°$ range representing physiossorption and chemosorption, 5–10 kJ·mol^{-1} and 30–40 kJ·mol^{-1}, respectively. Thus, it can be inferred that the adsorption process is not completely physical or chemical and that it occurs by more complex mechanisms [53,59].

Entropy variation ($\Delta S°$) predicts a measure of binding or repulsion forces in the system and is associated with the spatial arrangement of the adsorbate–adsorbent interface [60]. The positive value obtained for BCox (60 J·mol^{-1}·K^{-1}) indicates that entropy increases with the adsorption process, which may be related to the higher affinity between GLP-BCox than GLP-liquid medium, so that during the adsorption process, there is an increase in randomness in the solid–liquid interface [61]. The negative value obtained for BC (–70 J·mol^{-1}·K^{-1}) implies that GLP in the liquid sinus (aqueous solution) presents a more chaotic distribution when compared to the ordered state in the solid phase (BC surface) [62]. These values could explain the higher adsorption capacity of GLP in BCox than in BC, since the latter had lower affinity for adsorbate.

The $\Delta G > 0$ values for BC and BCox indicate that the GLP adsorption process was not thermodynamically spontaneous, and the results obtained are considered low (5–40 kJ·mol^{-1}) characterizing processes governed by physiossorption mechanisms.

4. Conclusion

The pH and adsorbent mass were determinants of GLP adsorption. Both adsorbents reached their maximum adsorption capacity at neutral pH (7.0).

Oxidation with H_3PO_4 caused a decrease in the surface area of BCox when compared to BC and did not produce micropores. It was also verified that oxidation did not significantly alter the functional groups present on the surface of the adsorbent material but rather the amount present, such as the case of functional groups containing oxygen in BCox.

Although the adsorption process occurs at rates considered adequate, the adsorption capacity of both adsorbents can be considered low, even after acid oxidation.

The adsorption balance was 60 min for both BC and BCox, with adsorption capacities of 0.58 mg·g^{-1} (22.3%) for BC and 1.49 mg·g^{-1} (53.2%) for BCox; however, BCox presented a higher initial adsorption speed, reaching 44% removal in the first 5 min, while BC was 5%.

The pseudo-first-order model adjusted adequately for both adsorbents; however, for BCox, the Avrami model suggested that adsorption also occurs according to the pseudo-second-order model. The results obtained indicate that both in BC and BCox, GLP adsorption is controlled by the external mass transfer coefficient and dependent on the initial GLP concentration. The values of k_1 for the BC of 0.06361 min^{-1} and for the BCox of 0.34698 min^{-1} (~5.4 times higher) confirm the higher GLP adsorption speed in BCox.

For BC, the Langmuir model was the one that best fit the GLP adsorption data, and for BCox, the most appropriate was the Freundlich model, which was not able to adjust the Langmuir model. The data suggest that adsorption occurred both by physical and chemical interactions.

The thermodynamic parameters confirmed that for both adsorbents, adsorption was an endothermic and non-spontaneous phenomenon. Entropy values show that GLP had a higher affinity with BCox than with BC.

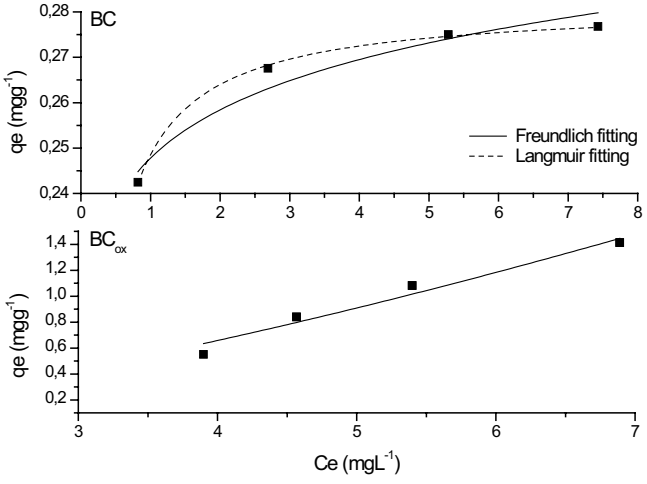

Fig. 9. Adjustment of GLP adsorption capacity data in BC and BCox to Langmuir and Freundlich adsorption isotherm models. *Notes*: Orbital agitation at 120 rpm, 4 h, pH = 7.0, temperature of 23°C, triplicate.

References

[1] G.A. Khoury, T.C. Gehris, L. Tribe, R.M. Torres Sánchez, M.S. dos Santos Afonso, Glyphosate adsorption on montmorillonite: an experimental and theoretical study of surface complexes, Appl. Clay Sci., 50 (2010) 167–175.

[2] J. Rendon-von Osten, R. Dzul-Caamal, Glyphosate residues in groundwater, drinking water and urine of subsistence farmers from intensive agriculture localities: a survey in Hopelchén, Campeche, Mexico, Int. J. Environ. Res. Public Health, 14 (2017) 595–608.

[3] F. Braghiroli, H. Bouafif, C. Neculita, A. Koubaa, Activated biochar as an effective sorbent for organic and inorganic contaminants in water, Water Air Soil Pollut., 229 (2018) 1–22.

[4] M.N. Rashed, Adsorption Technique for the Removal of Organic Pollutants from Water and Wastewater, M. Nageeb Rashed, Ed., Organic Pollutants-Monitoring, Risk and Treatment, InTechOpen, 2013, pp. 167–194.

[5] M. Ahmad, S.S. Lee, A.U. Rajapaksha, M. Vithanage, M. Zhang, J.S. Cho, S.E. Lee, K.S. Ok, Trichloroethylene adsorption by pine needle biochars produced at various pyrolysis temperatures, Bioresour. Technol., 143 (2013) 615–622.

[6] B. Sajjadi, T. Zubatiuk, D. Leszczynska, J. Leszczynski, W.Y. Chen, Chemical activation of biochar for energy and environmental applications: a comprehensive review, Rev. Chem. Eng., 35 (2019) 777–815.

[7] W.J. Liu, H. Jiang, H.Q. Yu, Development of biochar-based functional materials: toward a sustainable platform carbon material, Chem. Rev., 115 (2015) 12251–12285.

[8] K.A. Thompson, K.K. Shimabuku, J.P. Kearns, D.R.U. Knappe, R.S. Summers, S.M. Cook, Environmental comparison of biochar and activated carbon for tertiary wastewater treatment, Environ. Sci. Technol., 50 (2016) 11253–11262.

[9] Q.A. Binh, H. Nguyenb, Investigation the isotherm and kinetics of adsorption mechanism of herbicide 2,4-dichlorophenoxyacetic

acid (2,4-D) on corn cob biochar, Bioresour. Technol. Rep., 11 (2020) 100520, doi: 10.1016/j.biteb.2020.100520.
[10] A.S.I.A. Magid, I.M. Shafiqul, C. Yali, W. Liping, S. Yang, C. Xingping, Z. Bin, M. Jie, L. Yongtao, Competitive adsorption of dibutyl phthalate (DBP) and di(2-ethylhexyl) phthalate (DEHP) onto fresh and oxidized corncob biochar, Chemosphere, 280 (2021) 130639, doi: 10.1016/j.chemosphere.2021.130639.
[11] B.S. Giri, S. Gun, S. Pandey, A. Trivedi, R.T. Kapoor, R.P. Singh, O.M. Abdelbayem, E.R. Rene, S. Yadav, P. Chaurvedi, N. Sharma, R.S. Singh. Reusability of brilliant green dye contaminated wastewater using corncob biochar and *Brevibacillus parabrevis*: hybrid treatment and kinetic studies, Bioengineered, 11 (2020) 743–758.
[12] T. Suwunwong, N. Hussain, S. Chantrapromma, K. Phoungthong, Facile synthesis of corncob biochar via in-house modified pyrolysis for removal of methylene blue in wastewater, Mater. Res. Express, 7 (2020) 15518.
[13] J. Wang, S. Wang, Preparation, modification and environmental application of biochar: a review, J. Cleaner Prod., 227 (2019) 1002–1022.
[14] L. Zhu, N. Zhao, L. Tong, Y. Lv, G. Li, Characterization and evaluation of surface modified materials based on porous biochar and its adsorption properties for 2,4-dichlorophenoxyacetic acid, Chemosphere (Oxford), 210 (2018) 734–744.
[15] J. Alcañiz-Monge, M.C. Román-Martínez, M.Á. Lillo-Ródenas, Chemical activation of lignocellulosic precursors and residues: what else to consider?, Molecules (Basel, Switzerland), 27 (2022) 1630, doi: 10.3390/molecules27051630.
[16] J.S. Cha, S.H. Park, S.H. Jung, C. Ryu, J.K. Jeon, M.C. Shin, Y.K. Park, Production and utilization of biochar: a review, J. Ind. Eng. Chem. (Seoul, Korea), 40 (2016) 1–15.
[17] G. Chu, J. Zhao, Y. Huang, D. Zhou, Y. Liu, M. Wu, H. Peng, Q. Zhao, B. Pan, C.E.W. Steinberg, Phosphoric acid pretreatment enhances the specific surface areas of biochars by generation of micropores, Environ. Pollut., 240 (2018) 1–9.
[18] Q. Meng, Y. Zhang, D. Meng, X. Liu, Z. Zhang, P. Gao, A. Lin, L. Hou, Removal of sulfadiazine from aqueous solution by in situ activated biochar derived from cotton shell, Environ. Res., 191 (2020) 110104, doi: 10.1016/j.envres.2020.110104.
[19] Y. Ma, P. Li, L. Yang, L. Wu, L. He, F. Gao, X. Qi, Z. Zhang, Iron/zinc and phosphoric acid modified sludge biochar as an efficient adsorbent for fluoroquinolones antibiotics removal, Ecotoxicol. Environ. Saf., 196 (2020) 110550, doi: 10.1016/j.ecoenv.2020.110550.
[20] H.H. Cho, K. Wespasnick, B.A. Smith, F.K. Bangash, D.H. Fairbrother, W.P. Ball, Sorption of aqueous Zn[II] and Cd[II] by multiwall carbon nanotubes: the relative roles of oxygen-containing functional groups and graphenic carbon, Langmuir, 26 (2010) 967–981.
[21] K. Sen, J.K. Datta, N.K. Mondal, Glyphosate adsorption by *Eucalyptus camaldulensis* bark/mediated char and optimization through response surface modeling, Appl. Water Sci., 9 (2019) 162, doi: 10.1007/s13201-019-1036-3.
[22] J. Iqbal; B.M. Al Hajeri, N.S. Shah, K. Wilson, C. Xavier, J. Shaalan, A.A. Al-Taani, F. Howari, Y. Nazzal, Preparation of H_3PO_4 modified Sidr biochar for the enhanced removal of ciprofloxacin from water, Int. J. Phytorem., 24 (2022) 1231–1242.
[23] N. Farhaneem, M.F. Dimin, A. Shaaban, N. Mohamad, Optimization of phosphoric acid treatment biochar using response surface method, Int. J. Adv. Manuf. Technol., 12 (2018) 453–466.
[24] S.S. Mayakaduwa, P. Kumarathilaka, I. Herath, M. Ahmad, M. Al-Wabel, Y.S. Ok, A. Usman, A. Abduljabbar, M. Vithanage, Equilibrium and kinetic mechanisms of woody biochar on aqueous glyphosate removal, Chemosphere (Oxford), 144 (2016) 2516–2521.
[25] X. Jiang, Z. Ouyang, Z. Zhang, C. Yang, X. Li, Z. Dang, P. Wu, Mechanism of glyphosate removal by biochar supported nano-zero-valent iron in aqueous solutions, Colloids Surf., A, 547 (2018) 64–72.
[26] G. Herath, D. Anjali, L.S. Poh, W.J. Ng, Statistical optimization of glyphosate adsorption by biochar and activated carbon with response surface methodology, Chemosphere (Oxford), 227 (2019) 533–540.
[27] Y. Rajesh, U. Ramagopal, Effect of surfactant and sonication on Pd(II) adsorption from synthetic electroless plating solutions using commercial activated charcoal adsorbent, Desal. Water Treat., 57 (2016) 26073–26088.
[28] M. Nourouzi, M.T.G. Chuah, T.Y. Choong, Adsorption of glyphosate onto activated carbon derived from waste newspaper, Desal. Water Treat., 24 (2010) 321–326.
[29] P.F. De Sales, A.C. Bertoli, F.M. Pinto, Z.M. Magriotis, Produção, Caracterização e Aplicação do Carvão Ativado Obtido a partir do Sabugo De Milho: a busca pelo reaproveitamento de um resíduo agroindustrial, Rev. Virtual Quim., 7 (2015) 1174–1188.
[30] D.F. Tzaskos, C. Marcovicz, N.M.P. Dias, N.D. Rosso, Development of sampling for quantification of glyphosate in natural waters, Ciênc. Agrotec., 36 (2012) 399–405.
[31] P. Marin, B.C.E. Wudich, A.N. Módenes, S.P.D. Oliveira, L.S. Figueiredo, N. Passaia, Avaliação do Efeito da Temperatura, pH e Granulometria do Adsorvente na Adsorção do Corante Azul Reativo 5G, Engevista, 17 (2015) 59–68.
[32] J. Park, J.R. Regalbuto, A simple, accurate determination of oxide PZC and the strong buffering effect of oxide surfaces at incipient wetness, J. Colloid Interface Sci., 175 (1995) 239–252.
[33] K.E. Hall, K.A. Spokas, B. Gamiz, L. Cox, S.K. Papiernik, W.C. Koskinen, Glyphosate sorption/desorption on biochars–interactions of physical and chemical processes, Pest Manage. Sci., 74 (2018) 1206–1212.
[34] G.L. Dotto, L.G. Vieira, L.A.A. Pinto, Kinetics and mechanism of tartrazine adsorption onto chitin and chitosan, Ind. Eng. Chem. Res., 51 (2012) 6862–6868.
[35] Y. Deng, M. Li, Z. Zhang, Q. Liu, K. Jiang, J. Tian, Y. Zhang, F. Ni, Comparative study on characteristics and mechanism of phosphate adsorption on Mg/Al modified biochar, J. Environ. Chem. Eng., 9 (2021) 105079, doi: 10.1016/j.jece.2021.105079.
[36] K.C. Castro, A.S. Cossolin, H.C.O. Reis, E.B. Morais, Biosorption of anionic textile dyes from aqueous solution by yeast slurry from brewery, Braz. Arch. Biol. Technol., 60 (2017) 1–13.
[37] Y.S. Ho, C.C. Wang, Sorption equilibrium of mercury onto ground-up tree fern, J. Hazard. Mater., 156 (2008) 398–404.
[38] F. Güzel, H. Sayğili, S.G. Akkaya, F. Koyuncu, Y. Cumal, Optimal oxidation with nitric acid of biochar derived from pyrolysis of weeds and its application in removal of hazardous dye methylene blue from aqueous solution, J. Cleaner Prod., 144 (2017) 260–265.
[39] K.S.W. Sing, Reporting physisorption data for gas/solid systems with special reference to the determination of surface area and porosity (Recommendations 1984), Pure Appl. Chem., 57 (1985) 603–619.
[40] D.M. Ruthven, Principles of Adsorption and Adsorption Process, John Wiley & Sons, New York, 1984.
[41] C.R. Zhou, G.P. Li, D.G. Jiang, Study on behavior of alkalescent fiber FFA-1 593 adsorbing glyphosate from production wastewater of glyphosate, Fluid Phase Equilib., 362 (2014) 69–73.
[42] F. Ates, O. Özcan, Preparation and characterization of activated carbon from poplar sawdust by chemical activation: comparison of different activating agents and carbonization temperature, Eur. J. Eng. Technol. Res., 3 (2018) 6–11.
[43] Suhas, P.J.M. Carrott, M.M.L.R. Carrott, R. Singh, L.P. Singh, M. Chaudhary, An innovative approach to develop microporous activated carbons in oxidizing atmosphere, J. Cleaner Prod., 156 (2017) 549–555.
[44] I. Herath, P. Kumarathilaka, M.I. Al-Wabel, A. Abduljabbar, M. Ahmad, A.R.A. Usman, M. Vithanage, Mechanistic modeling of glyphosate interaction with rice husk derived engineered biochar, Microporous Mesoporous Mater., 225 (2016) 280–288.
[45] P. Kumar, H. Singh, M. Kapur, M.K. Mondal, Comparative study of Malathion removal 605 from aqueous solution by agricultural and commercial adsorbents, J. Water Process Eng., 3 (2014) 67–73.
[46] N.U. Yamaguchi, R. Bergamasco, S. Hamoudi, Magnetic $MnFe_2O_4$-graphene hybrid composite for efficient removal of glyphosate from water, Chem. Eng. J., 295 (2016) 391–402.

[47] S.M. Yakout, G.S. El-Deen, Characterization of activated carbon prepared by phosphoric acid activation of olive stones, Arabian J. Chem., 9 (2011) S1155–S1162.
[48] H. Zeng, H. Zeng, H. Zhang, A. Shahab, K. Zhang, Y. Lu, I. Nabi, F. Naseem, H. Ullah, Efficient adsorption of Cr(VI) from aqueous environments by phosphoric acid activated eucalyptus biochar, J. Cleaner Prod., 286 (2021) 124964, doi: 10.1016/j.jclepro.2020.124964.
[49] O. Yang, P. Wu, J. Liu, S. Rehman, Z. Ahmed, B. Ruan, N. Zhu, Batch interaction of emerging tetracycline contaminant with novel phosphoric acid activated corn straw porous carbon: adsorption rate and nature of mechanism, Environ. Res., 181 (2020) 108899, doi: 10.1016/j.envres.2019.108899.
[50] Z. Lu, H. Zhang, A. Shahab, K. Zhang, H. Zeng, A.Z.U.R. Bacha, I. Nabi, H. Ullah, Comparative study on characterization and adsorption properties of phosphoric acid activated biochar and nitrogen-containing modified biochar employing Eucalyptus as a precursor, J. Cleaner Prod., 303 (2021) 127046, doi: 10.1016/j.jclepro.2021.127046.
[51] R. Yang, G. Liu, X. Xu, M. Li, J. Zhang, X. Hao, Surface texture, chemistry and adsorption properties of acid blue 9 of hemp (*Cannabis sativa* L.) bast-based activated carbon fibers prepared by phosphoric acid activation, Biomass Bioenergy, 35 (2011) 437–631.
[52] H. Niu, H. Jin, Q. Sun, Y. Shi, X. Zhang, Y. Cai, Activation of biochars by waste phosphoric acids: an integrated disposal route of waste acids and solid waste, ACS Sustainable Chem. Eng., 9 (2021) 16403–16414.
[53] N.U. Yamaguchi, A.J. Rubio, R. Bergamasco, Carvão Ativado Impregnado com Manganês e Ferro para Adsorção de Glifosato: Cinética, isotermas e estudos termodinâmicos, Rev. Ambient e Água, 14 (2019) 1–6.
[54] M. Reck, R.M. Paixão, R. Bergamasco, M.F. Vieira, A.M.V. Salcedo, Removal of tartrazine from aqueous solutions using adsorbents based on activated carbon and *Moringa oleifera* seeds, J. Cleaner Prod., 171 (2018) 85–97.
[55] S. Chen, C. Qin, T. Wang, F. Chen, X. Li, H. Hou, M. Zhou, Study on the adsorption of dyestuffs with different properties by sludge-rice husk biochar: adsorption capacity, isotherm, kinetic, thermodynamics and mechanism, J. Mol. Liq., 285 (2019) 62–74.
[56] M.D.G. De Luna, M.F. Divinagracia, A.E.C. Sy, D.C. Ong, W. Chung, Applicability of composite silica–divinylbenzene in bioethanol dehydration: equilibrium, kinetic, thermodynamic, and regeneration analysis, Energy Fuels, 33 (2019) 7347–7356.
[57] T. Akar, A.S. Ozcan, S. Tunali, A. Ozcan, Biosorption of a textile dye (acid blue 40) by cone biomass of *Thuja orientalis*: estimation of equilibrium, thermodynamic and kinetic parameters, Bioresour. Technol., 99 (2008) 3057–3065.
[58] P. Zhang, Y. Li, Y. Cao, L. Han, Characteristics of tetracycline adsorption by cow manure biochar prepared at different pyrolysis temperatures, Bioresour. Technol., 285 (2019) 121348, doi: 10.1016/j.biortech.2019.121348.
[59] F.X. Chen, C.R. Zhou, G.P. Li, F.F. Peng, Thermodynamics and kinetics of glyphosate adsorption on Resin D301, Arabian J. Chem., 9 (2016) S1665–S1669.
[60] M. Vithanage, S.S. Mayakaduwa, I. Herath, Y.S. Ok, D. Mohan, Kinetics, thermodynamics and mechanistic studies of carbofuran removal using biochars from tea waste and rice husks, Chemosphere (Oxford), 150 (2015) 781–789.
[61] I.A.W. Tan, B.H. Hameed, A.L. Ahamed, Equilibrium and kinetic studies on basic dye 568 adsorption by oil palm fibre activated carbon, Chem. Eng. J., 127 (2007) 111–119.
[62] N. Azouaou, Z. Sadaoui, A. Djaafri, H. Mokaddem, Adsorption of cadmium from aqueous 661 solution onto untreated coffee grounds: equilibrium, kinetics and thermodynamics, J. Hazard. Mater., 184 (2010) 126–134.